Journal of Manufacturing Processes 62 (2021) 108–118

Contents lists available at ScienceDirect

Journal of Manufacturing Processes

journal homepage: www.elsevier.com/locate/manpro

One-step fabrication of regular hierarchical micro/nano-structures on glassy carbon by nanosecond pulsed laser irradiation

Chao Wang [a], Hu Huang [a,*], Yongfeng Qian [a], Zhiyu Zhang [b], Jiwang Yan [c]

[a] Key Laboratory of CNC Equipment Reliability, Ministry of Education, School of Mechanical and Aerospace Engineering, Electron Microscopy Center, Jilin University, Changchun, Jilin, 130022, China
[b] Key Laboratory of Optical System Advanced Manufacturing Technology, Changchun Institute of Optics, Fine Mechanics and Physics, Chinese Academy of Sciences, Changchun, China
[c] Department of Mechanical Engineering, Faculty of Science and Technology, Keio University, Yokohama, 223-8522, Japan

ARTICLE INFO

Keywords:
Glassy carbon
Nanosecond pulsed laser
Ring-like nanostructure
Wettability

ABSTRACT

Fabrication of hierarchical micro/nano-structures on glassy carbon (GC) surface is important for the application of GC as the mold material for glass molding, but it is still challenging due to the high brittleness and hardness of the material. In this study, by using a nanosecond pulsed laser, a hierarchical micro/nano-structure, i.e., micro-dimple with ring-like nanostructure on its inner wall, was generated on the GC surface. The effects of laser parameters, such as laser irradiation time and fluence, on the formation and evolution of the hierarchical micro/nano-structure were experimentally studied. By comparative experiments with graphite, the role of amorphous nature of GC on the formation of very regular hierarchical micro/nano-structure was confirmed. The results obtained by irradiating GC in argon and nitrogen gas further indicated that the formation of hierarchical micro/nano-structure was independent of the gas atmosphere. By controlling the relative positions of point shots, various micro-dimple arrays were successfully fabricated on the GC surface which significantly changed its wetting behavior. Finally, formation mechanism of the hierarchical micro/nano-structure was discussed according to the experimental results as well as some previous literatures. This study provides a one-step method for fabricating hierarchical micro/nano-structures on the GC surface by nanosecond pulsed laser irradiation, which would be meaningful for the functional applications of GC.

1. Introduction

With a disordered atomic structure, glassy carbon (GC) exhibits isotropic mechanical, physical, and chemical properties. On the one hand, it possesses the common characteristics of carbon materials, such as good thermal stability and excellent electrical conductivity [1,2]. On the other hand, GC also shows some unique properties such as high strength, high elasticity, low density, low thermal expansion, and extreme corrosion resistance. With these features, GC is generally employed as electrode materials in the field of analytical chemistry [3,4], and as well, it is widely used as thermal imprinting molds for precision glass molding [5].

For applications as a mold, fabrication of some specific surface structures on GC is the first step. However, due to the high brittleness and hardness of GC, the conventional machining methods unavoidably resulted in poor surface quality, and defects were commonly observed on the machined surface [6]. Even though these surface defects could be partially reduced by using some hybrid machining methods [6,7], they could not be completely eliminated. For example, micro-fractures still existed on the GC surface after ultrasonic vibration-assisted micro-grinding [7]. Alternatively, several non-mechanical approaches have been explored in some previous studies. For example, by combining femtosecond laser ablation with subsequent focused ion beam (FIB) milling, Youn et al. [8] provided a method to fabricate microstructures on the GC surface with relatively high quality and efficiency, compared to that when using either of femtosecond laser ablation or FIB milling. Later, they combined the electron beam lithography (EBL) with reactive ion etching (RIE) to prepare the GC molds, which were applicable for thermal imprinting of kinds of materials [9]. Kim et al. [10] reported the preparation of GC mold with microdome cavities by carbonization of a furan precursor, and they further copied the microdome structure to an aluminum plate by using direct metal molding. Laser processing itself as

* Corresponding author.
E-mail address: huanghu@jlu.edu.cn (H. Huang).

https://doi.org/10.1016/j.jmapro.2020.12.043
Received 28 August 2020; Received in revised form 11 December 2020; Accepted 13 December 2020
Available online 24 December 2020

a versatile technology has also been applied to fabricate the GC molds [11,12]. For example, by using a nanosecond pulsed Yb fiber laser, various structures such as microprobe and trench structures were machined on the GC surface, which worked as a master mold for subsequent soft lithography [11]; similarly, by using ultraviolet laser milling, micro-fluidic channels were prepared on the GC surface and it was further applied to hot stamping of soda-lime glass [12].

Although various microstructures have been successfully fabricated on the GC surfaces by the above-mentioned processing methods, the formed structures were single-scale ones. Many previous studies suggested that compared to the single-scale structure, hierarchical micro/nano-structures could readily endow the surface with some unique properties, for example, tuning the hydrophobicity or hydrophilcity [13–16], enhancing the light absorption efficiency [17], promoting dropwise condensation [18] and drop motion [19], suppressing frost and promoting defrost [20], improving tribological performance [21,22], and so on. However, fabrication of hierarchical micro/nano-structures on the GC surface is still challenging, so new processing methods should be further explored.

Compared to FIB milling, EBL, RIE, and femtosecond laser machining, nanosecond pulsed laser processing is less expensive and more efficient, and it has been widely employed to texture various materials [23–26]. Because of the complex interaction between the nanosecond pulsed laser and the material, not only micro-dimple or micro-groove but also nanoparticles and micro-clusters could be generated on the irradiated surface, forming typical hierarchical micro/nano-structures [27–30]. On the other hand, direct laser interference patterning also provides the possibility to prepare hierarchical micro/nano-structures [31,32]. Furthermore, with some additional physical effects such as light interference or thermoplastic extrusion, more specific hierarchical micro/nano-structures have been reported by nanosecond pulsed laser irradiation [33–35]. Accordingly, in this study, we attempted to develop a one-step method for fabricating hierarchical micro/nano-structures on the GC surface by nanosecond pulsed laser irradiation. Via point shot, the micro-dimple with ring-like nanostructure on its inner wall, was successfully generated on the GC surface, and the formation of ring-like nanostructure strongly depended on the laser irradiation time and fluence. Using the selected laser parameters, regular micro-dimple arrays were fabricated on the GC surface, and their effect on the surface wettability was further characterized. According to the experimental results as well as some previous studies, formation mechanism of the hierarchical micro/nano-structure was finally discussed.

2. Materials and experiments

Glassy carbon bought from the company, UNITIKA LTD., Japan, was employed as the experimental sample, which had been polished by the company. Prior to laser irradiation, the sample was cleaned using ethanol and the amorphous nature of GC was confirmed by using an NRS-3000 Raman micro-spectrometer (JASCO, Japan) with a 532 nm wavelength laser.

Laser irradiation was performed in air via a nanosecond pulsed laser (SP-050P-A-EP-Z-F-Y, SPI, UK). It is a fiber laser with a wavelength of 1064 nm and a Gaussian beam (TEM_{00} mode, $M^2 < 1.6$) focused to be a spot with the diameter of ~42 μm. During experiments, a repetition frequency of 700 kHz was employed, and the corresponding laser pulse width was 7 ns. By preliminary experiments, the maximum single pulse energy used in subsequent experiments was 0.05 mJ. Point shots under various laser irradiation times and fluences were first conducted to study the effects of laser parameters on the surface structures, followed by fabricating large-area array structures on the GC surface using the selected laser parameters. The detailed experimental parameters are listed in Table 1. For comparison, laser irradiation was also performed on the graphite plate as well as in argon and nitrogen atmospheres.

After laser irradiation, surface topography was characterized by using a laser scanning confocal microscopy (LSCM, OLS4100, Olympus, Japan), and surface morphology was observed by using a tungsten filament scanning electron microscope (SEM, JSM-IT500A, JEOL, Japan). During SEM observation, the acceleration voltage, current, and working distance (WD) were 5.0 kV, 3.0 mA, and 10.1 mm, respectively. The wettability of the original GC surface as well as the structured surface was characterized by a contact angle measuring instrument (OAS60, NBSI, China), and the droplet volume for measurement was 2 μL.

Table 1
The detailed experimental parameters for point shot.

Sample material	Glassy carbon (GC)
Irradiation time (ms)	0.4, 0.8, 1.0, 1.2, 1.6, 2.0
Laser fluence (J/cm^2)	0.210, 0.226, 0.235, 0.257, 0.270
Laser repetition frequency (kHz)	700
Laser pulse width (ns)	7

3. Results and discussion

3.1. Confirmation of the amorphous nature of GC

Fig. 1 shows the Raman spectrum of GC in the range of 800 to 1800 cm^{-1}, where two typical peaks are observed, the D peak at about 1360 cm^{-1} and the G peak at around 1590 cm^{-1}. The D peak is related to the defect concentration (or "disorder") of the crystal lattice, and the G peak is associated with the graphitic or "ordered" domains in carbon material. Generally, the intensity ratio (I_D/I_G) is employed to evaluate the degree of graphitization or amorphization of carbon materials [36,37]. The intensity of D peak is larger than that of G peak ($I_D/I_G > 1$), agreeing well with the typical GC peaks in some previous literatures [38,39]. Therefore, the Raman spectrum in Fig. 1 confirms the amorphous nature of the used GC.

3.2. Formation of single micro-dimple

Fig. 2(a) presents the optical morphology of the GC surface after point shot under the laser fluence of 0.235 J/cm^2 and irradiation time of 1.0 ms. Fig. 2(b) shows the profile of the dotted line marked in Fig. 2(a). Fig. 2(c) and (d) are the corresponding three-dimensional (3D) topographies in different views. It is clearly seen that under the employed experimental parameters, two kinds of surface structures have been generated on the GC surface, one is the micro-dimple and the other is the

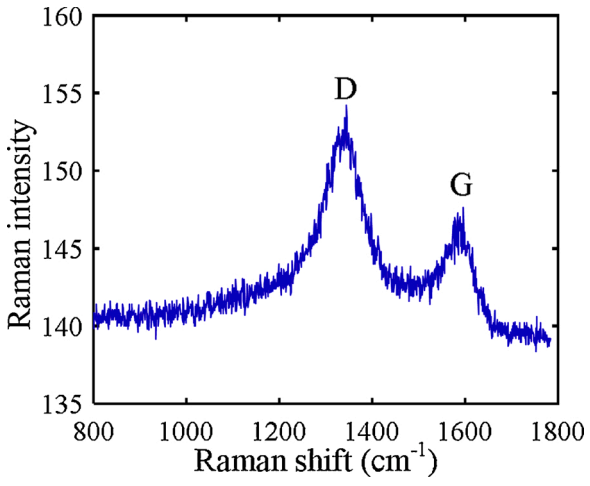

Fig. 1. Raman spectrum of the GC sample obtained in the range of 800 to 1800 cm^{-1}. The D peak appears at about 1360 cm^{-1} and the G peak appears at around 1590 cm^{-1}.

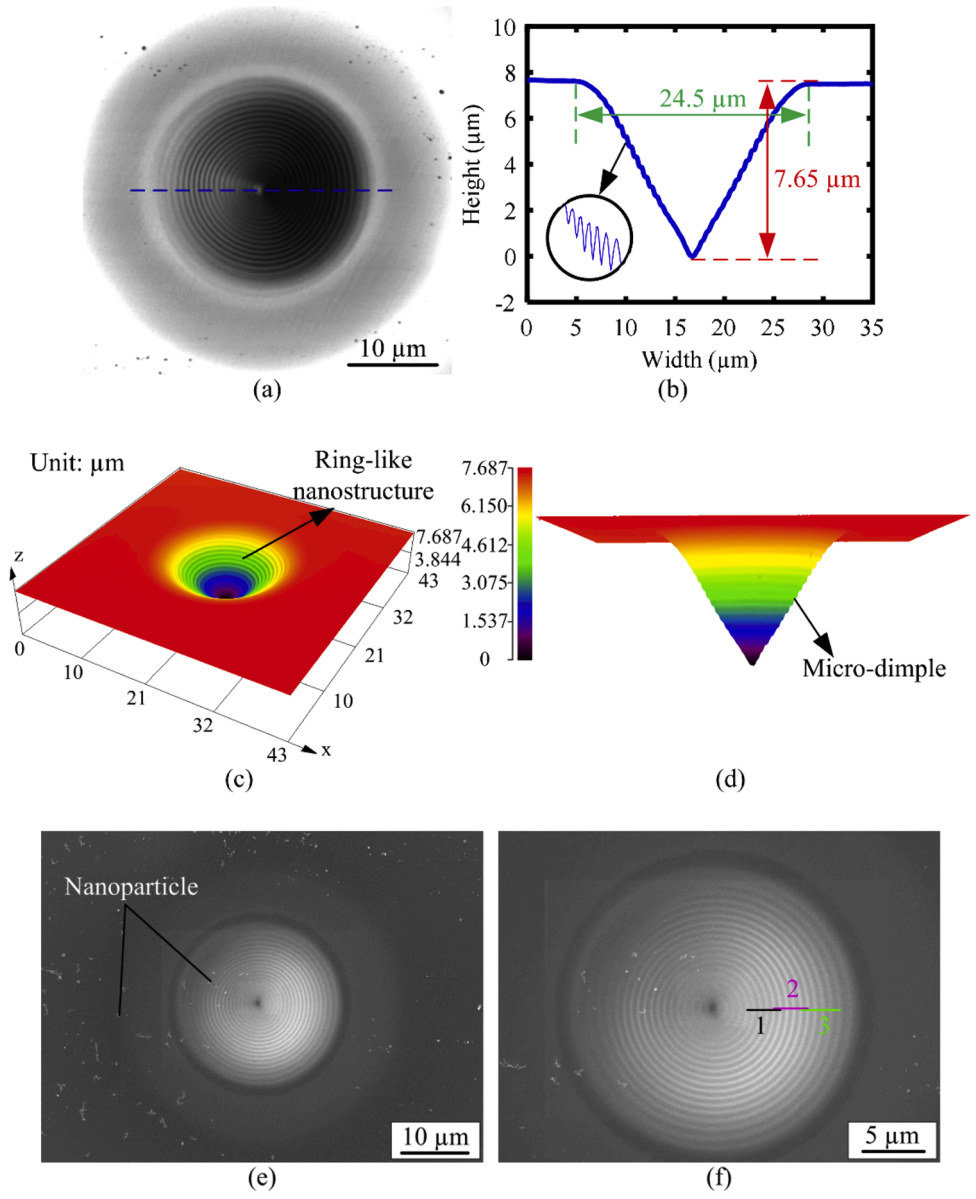

Fig. 2. (a) Optical morphology of the GC surface after point shot under the laser fluence of 0.235 J/cm^2 and irradiation time of 1.0 ms. (b) Profile of the dotted line in Fig. 2(a). (c) and (d) The corresponding three-dimensional (3D) topographies of Fig. 2(a) in different views. (e) and (f) SEM morphologies of the irradiated GC surface with different magnifications.

ring-like nanostructure. The micro-dimple has a depth of 7.65 μm and diameter of 24.5 μm. It is noted that the diameter of the micro-dimple is significantly less than that of the laser beam (~42 μm), which is due to the Gaussian energy distribution. For Gaussian beam, the laser energy intensity near the center is relatively high and it tends to decrease along the radial direction. According to some previous studies [40,41], the ablation threshold of the used GC was experimentally determined to be 0.150 J/cm^2. Under the laser fluence of 0.235 J/cm^2 here, the laser energy of the center region is over the ablation threshold, resulting in the formation of micro-dimple; while the laser energy of the surrounding region does not reach the ablation threshold and thus, only a circular heat affected zone (HAZ) is generated around the micro-dimple. From the cross-sectional profile in Fig. 2(b), very uniform and orderly concentric ring-like structure can be observed on the inner wall of the micro-dimple, which results in the inner wall being not smooth but jagged shape. Therefore, the formed surface structure after point shot is a typical hierarchical micro/nano-structure. The 3D topographies shown in Fig. 2(c) and 2(d) further confirm this, and both the micro-dimple and ring-like nanostructure can be clearly observed. From Fig. 2(b)–(d), it is also noted that the surface outside the micro-dimple is quite flat, nearly the same as the original surface. This is quite different from the surface characteristics of metal materials after laser point shot, where remarkable pile-up could be observed around the micro-dimple [42].

Fig. 2(e) and (f) present the corresponding SEM morphologies with different magnifications. It is further confirmed that the formed hierarchical micro/nano-structure on GC surface is quite regular and clean, with only some nanoparticles on and around it. In addition, from Fig. 2 (f), it is seen that the period of the ring-like nanostructure near the outer boundary seems a little larger than that of the ring-like nanostructure near the centre. As the ring-like nanostructure is distributed on the inner wall of the micro-dimple, it is difficult to directly measure its period because of the inclined inner wall. In Fig. 2(f), the ring-like nanostructure is projected on the horizontal plane; as the periods of the ring-like nanostructure and the projected one are directly proportional, the period of the projected one is used here. Accordingly, three lines (1, 2, and 3) are marked along the radial direction of the micro-dimple as

shown in Fig. 2(f), and each line covers five ring-like nanostructures. By comparing the length of lines 1–3 with that of the scale bar, three periods could be obtained, and they are 542 ± 5 nm, 558 ± 5 nm, and 632 ± 5 nm, respectively. This result indicates that the period of the ring-like nanostructure tends to slightly increase from the bottom to the top of the micro-dimple. The slight change in period of the ring-like nanostructure could be related to the slight change in slope of the cross-sectional profile from the bottom to the top as shown in Fig. 2(b).

To investigate the effects of laser parameters on the formation of the hierarchical micro/nano-structure, point shots were further performed under different laser irradiation times and fluences. Fig. 3 shows SEM morphologies obtained under various laser irradiation times but the same laser fluence of 0.235 J/cm^2. When the irradiation time is 0.4 ms, only micro-dimple has been formed in the ablated area, and the ring-like nanostructure does not appear. When gradually increasing the irradiation time, the ring-like nanostructure begins to appear, and it is gradually deepened with increase in the irradiation time. When the irradiation time is 1.0 ms, the ring-like nanostructure becomes the most regular and remarkable. Further increasing the irradiation time to 1.2 ms, wrinkles begin to appear on the inner wall of the micro-dimple, causing the ring-like nanostructure in the center area to deteriorate. When the irradiation time is increased to 1.6 ms, the wrinkles have extended outward along five directions, and the ring-like nanostructure in the central area has been damaged and become extremely irregular. When the irradiation time reaches 2.0 ms, the wrinkles tend to become shallower and a new kind of ring-like nanostructure has been generated in the central area. However, compared with the previous ring-like nanostructure, the period of the new ring-like structure becomes non-uniform. Apart from the evolution of hierarchical micro/nano-structure, the accompanied nanoparticles formed around the micro-dimple are evolved as well. Generally, when the irradiation times are less than 1.2 ms, very few nanoparticles are generated around the micro-dimple. When the irradiation time exceeds 1.2 ms, large-area nanoparticles have been formed around the micro-dimple as shown in Fig. 3(e) and (f).

To investigate the effect of laser irradiation time on the period of the ring-like nanostructure, the period of the ring-like nanostructure in the middle region of the inner wall is measured as an example. The similar method as shown in Fig. 2 is employed. For the laser irradiation time of 0.8 ms, 1.0 ms and 1.2 ms, the ring-like nanostructures are clear and regular, so these three cases are evaluated and the corresponding periods are calculated to be nearly the same (558 ± 5 nm). The comparative results in Fig. 3 indicate that the formation of hierarchical micro/nano-structure is significantly affected by the laser irradiation time. When the irradiation time is too short, the ring-like nanostructure will not be generated; when it is too long, the previously formed ring-like nanostructure will be damaged again. However, once the ring-like nanostructure has been formed, its period is nearly independent of the laser irradiation time.

Fig. 4 shows the effects of laser irradiation time on the diameter and depth of the micro-dimple. It is easy to find that with increase in the irradiation time, both the diameter and depth tend to increase. Furthermore, the increase in the depth direction is significantly larger than that in the radial direction. When the irradiation time is increased from 0.4 ms to 2.0 ms, the depth is increased from 1.5 μm to 15.0 μm, but the diameter is only increased from 19.8 μm to 28.0 μm. This could be explained as follows. When increasing the irradiation time, the HAZ near the ablated region could also reach the ablation threshold due to the heat accumulation of repeated laser shots, and thus the ablated diameter

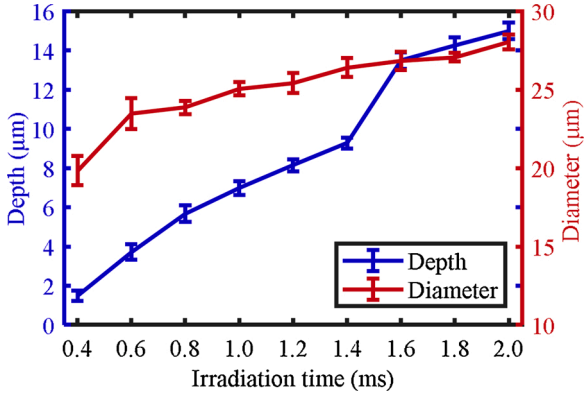

Fig. 4. Diameter and depth of the micro-dimple changing with the laser irradiation time. The laser fluence was kept to be 0.235 J/cm^2.

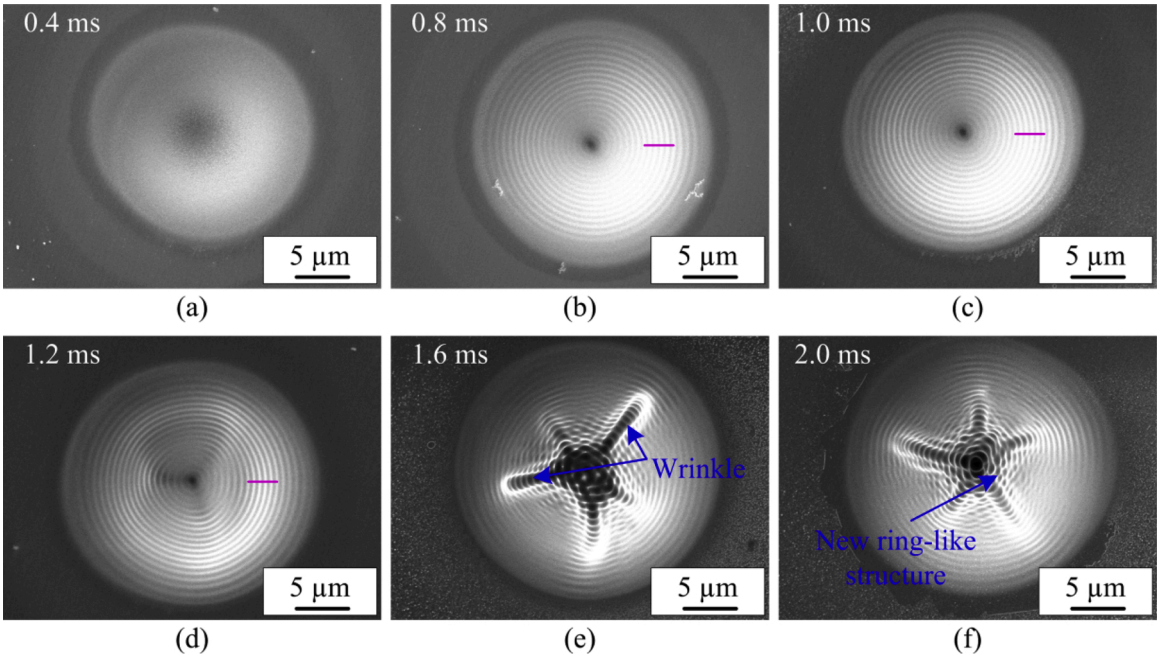

Fig. 3. SEM morphologies of the GC surface after point shot under various irradiation times: (a) 0.4 ms, (b) 0.8 ms, (c) 1.0 ms, (d) 1.2 ms, (e) 1.6 ms, and (f) 2.0 ms. The laser fluence was kept to be 0.235 J/cm^2.

gradually increases, resulting in the increase in diameter of the micro-dimple. Apart from the accumulated removal role of repeated laser shots when increasing the irradiation time, the preceding ablated surface could also greatly enhance the absorption of the laser energy during subsequent laser shot [43], which makes the subsequent ablation more severe and thus results in significant increase in depth of the micro-dimple.

Fig. 5 shows SEM morphologies of the GC surface after point shot under various laser fluences. The laser irradiation time was kept to be the same of 1.0 ms. It is noted that the effect of laser fluence on the hierarchical micro/nano-structure is very similar to that of laser irradiation time. Under a relatively low laser fluence, no ring-like nanostructure is generated on the inner wall of the micro-dimple; when gradually increasing the laser fluence, the ring-like nanostructure appears; the wrinkles finally occur and the regular ring-like nanostructure is damaged especially in the central area when the laser fluence is over a critical value. However, being different from the effect of laser irradiation time on the irradiated GC surface, there are less nanoparticles generated around the micro-dimple when similar wrinkles have been formed (comparing Fig. 3(e) with Fig. 5(d)).

To investigate the effect of amorphous nature of glassy carbon on the formation of hierarchical micro/nano-structure, point shots were further performed on the surface of graphite, which is a typical crystal material. As the effects of laser fluence and irradiation time are very similar as shown in Fig. 3 and 5, here the laser fluence was kept to be 0.235 J/cm^2, and the irradiation time was increased from 2.0 ms to 5.0 ms after preliminary experiments. Fig. 6 presents the SEM morphologies of graphite surface after point shot under various irradiation times. It is observed that when the irradiation time is less than 2.0 ms, only irregular micro-dimples are formed on the graphite surface; when the laser irradiation time reaches 3.0 ms, there are tendency to generate the ring-like nanostructure on the inner wall of the micro-dimple, but it is still very irregular, as shown in Fig. 6(b). With further increase in the irradiation time, the nanostructure on the inner wall is significantly damaged as shown in Fig. 6(c) and (d). Compared with GC, the formed micro-dimple on the graphite surface is quite irregular as well as the ring-like nanostructure, which could be due to the crystal anisotropy of graphite. The comparative results in Fig. 3 and 6 demonstrate that the amorphous nature of GC significantly contributes to the formation of very regular micro-dimple during laser point shot and subsequently the hierarchical micro/nano-structure.

3.3. Formation of various micro-dimple arrays

After investigating the dependence of hierarchical micro/nano-structure on the laser irradiation parameters by point shot, formation of various micro-dimple arrays on GC surface was further attempted by controlling the relative positions of point shots, which would be more meaningful for practical applications. Being different from point shot, another parameter, i.e. the interval between two adjacent micro-dimples was introduced for the fabrication of micro-dimple arrays. According to the results in section 3.2, the laser fluence of 0.235 J/cm^2 and irradiation time of 1.0 ms were employed for subsequent fabrication of micro-dimple arrays.

The first kind of micro-dimple arrays was constructed by using five points as a basic unit. As illustrated in Fig. 7(a) (the inserted image), this unit actually consists of two equilateral triangles which are symmetrically distributed. Fig. 7(a)–(c) show the 3D topographies of micro-dimple arrays formed under the intervals of 15, 20, and 25 μm, respectively. Fig. 7(d) illustrates the profiles of the dotted lines in each figure, showing the cross-sectional shape of each micro-dimple array. As shown in Fig. 7(a)–(c), very regular micro-dimple arrays have been formed, and each micro-dimple has the ring-like nanostructure on the inner wall. For Fig. 7(a) and (b), the intervals *d* between two adjacent micro-dimples (15 and 20 μm) are less than the diameter of the micro-dimples (24.5 μm) formed under this laser conditions according to Fig. 2. Therefore, the adjacent laser pulses will overlap the preceding ones, and thus, the saddle-shaped structure is formed in the interacted

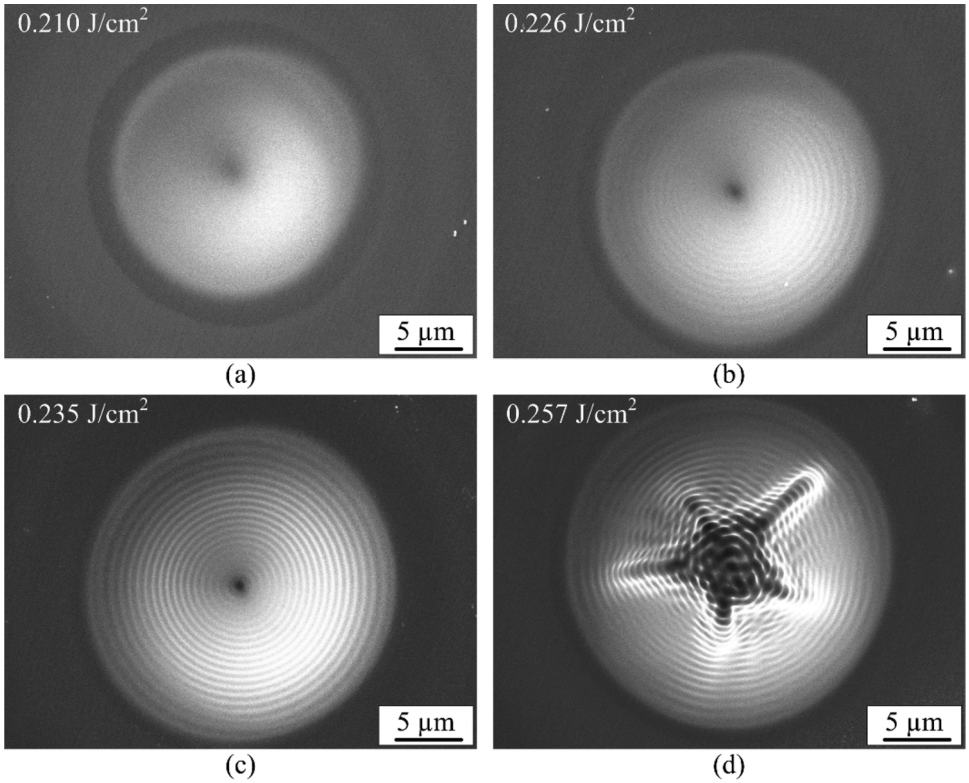

Fig. 5. SEM morphologies of the GC surface after point shot under various laser fluences: (a) 0.210 J/cm^2, (b) 0.226 J/cm^2, (c) 0.235 J/cm^2, and (d) 0.257 J/cm^2. The laser irradiation time was kept to be 1.0 ms.

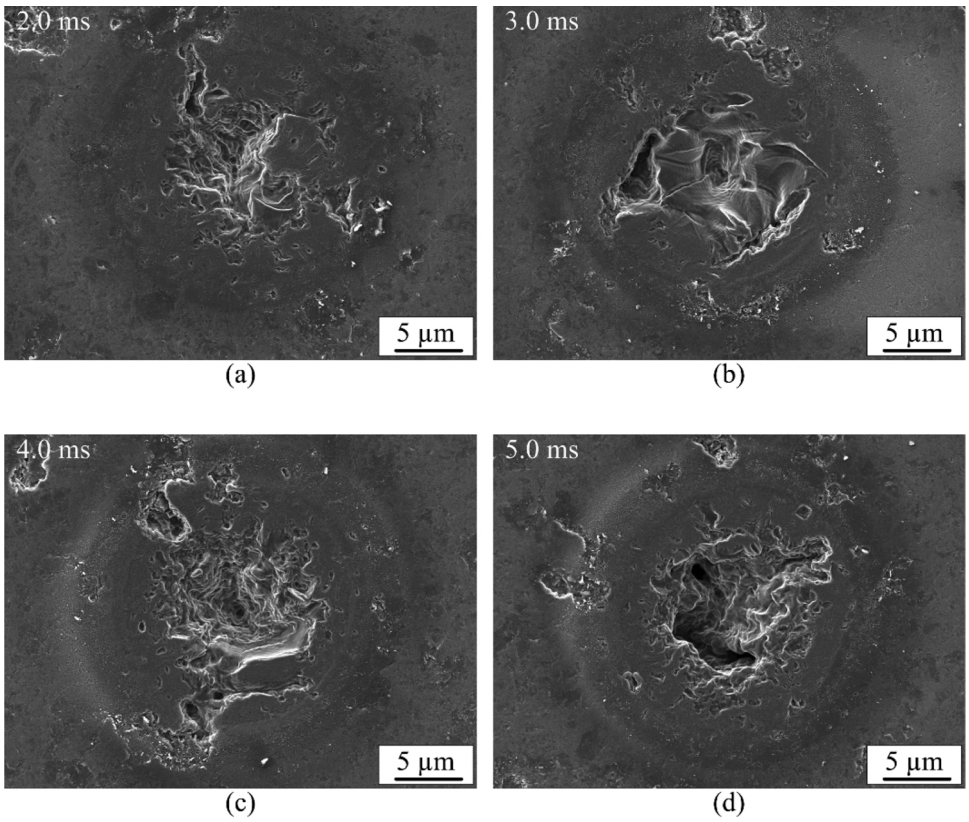

Fig. 6. SEM morphologies of graphite surface after point shot under various laser irradiation times: (a) 2.0 ms, (b) 3.0 ms, (c) 4.0 ms, and (d) 5.0 ms. The laser fluence was kept to be 0.235 J/cm^2.

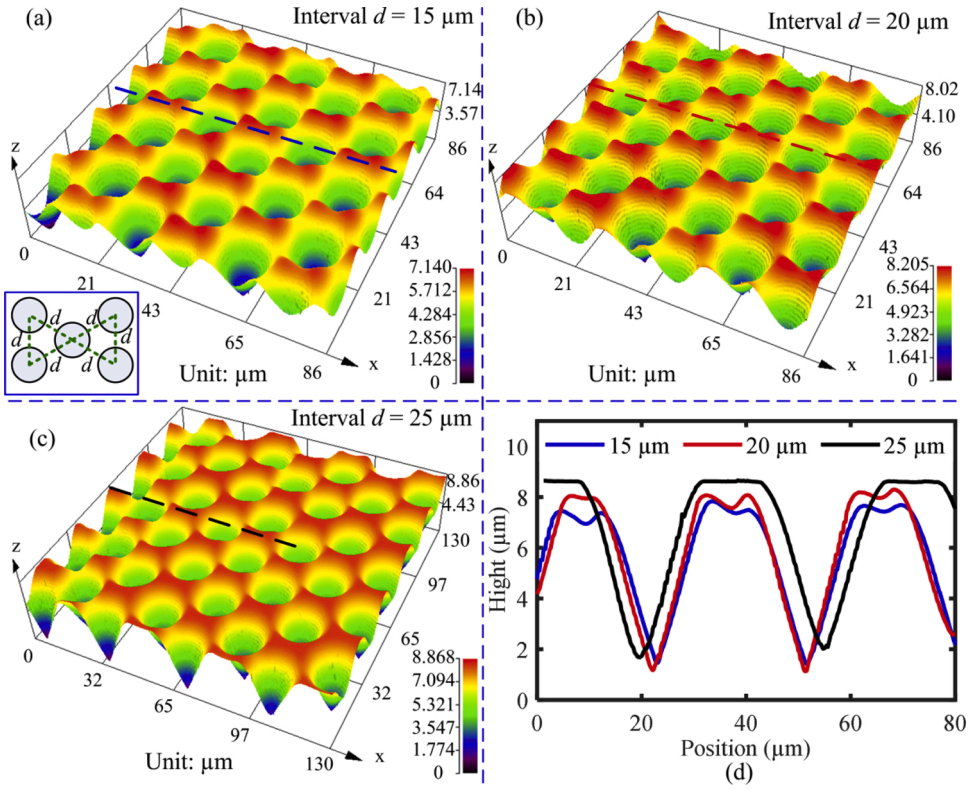

Fig. 7. 3D topographies of the micro-dimple arrays formed by using five points as a basic unit and controlling the interval: (a) d =15 μm, (b) d =20 μm, and (c) d =25 μm. (d) illustrates the profiles of the dotted lines in each figure.

region between two adjacent micro-dimples. For Fig. 7(c), the interval d between two adjacent micro-dimples (25 μm) is larger than the diameter of the formed micro-dimples (24.5 μm). Therefore, the individual micro-dimple could be clearly identified and there is nearly no direct interaction between two adjacent micro-dimples. The effect of interval on the surface topography could be further confirmed by analyzing the cross-sectional profiles as illustrated in Fig. 7(d). When the interval d is less than the diameter of the micro-dimple, the top of the profile is slightly wrinkled; while it is quite flat when the interval d is larger than the diameter of the micro-dimple. Fig. 8 presents the corresponding SEM morphologies, which further confirm the effect of interval on the formed micro-dimple array. In addition, the hierarchical micro/nano-structure is also confirmed from the SEM morphologies.

By controlling the relative positions of point shots, another two kinds of micro-dimple arrays were also attempted, which were constructed by using four and six points as a basic unit respectively, i.e. the square and hexagon shapes. Fig. 9 and 10 present the 3D topographies and SEM morphologies of the obtained micro-dimple arrays, respectively. It is noted that all the formed micro-dimple arrays are quite regular with ring-like nanostructure on the inner wall of each dimple, which are typical hierarchical micro/nano-structures. The results in Fig. 7–10 indicate that by simply changing the relative position and interval between adjacent points, various micro-dimple arrays could be easily fabricated on the GC surface. With consideration of the effects of laser fluence and irradiation time on the diameter and depth of the micro-dimple as shown in Fig. 4, the size of each micro-dimple in the micro-dimple array could be further tuned by changing the laser parameters.

Many previous studies [44–46] have demonstrated that surface microstructures especially the hierarchical micro/nano-structure could significantly alter the wetting behavior of material surfaces. Therefore, wettability of the fabricated micro-dimple arrays was preliminarily characterized by measuring the contact angle (CA). Fig. 11(a) shows the contact angle of the original GC surface and it is about 75°. Fig. 11(b)–(d) show the optical images and corresponding contact angles of the formed three kinds of micro-dimple arrays. It is clearly seen that the large-area micro-dimple arrays with various basic units have been successfully fabricated on the GC surface, and the structured surfaces significantly reduce the contact angle. Especially, the micro-dimple arrays with the hexagon-shaped basic unit show the superhydrophilic behavior with a contact angle of 7°. The other two kinds of micro-dimple arrays also have the contact angle of about 11°, being 64° less than that of the original GC surface. This comparison confirms that fabrication of hierarchical micro/nano-structures on the GC surface could significantly change its wetting behavior.

3.4. Formation mechanism of the hierarchical micro/nano-structure

For laser irradiation of GC in air, the interaction between the laser and GC surface should be quite complex due to the chemical reaction between the GC and oxygen in air. To explore the formation mechanism of the hierarchical micro/nano-structure, the role of chemical reaction should be first investigated. Accordingly, laser irradiation of GC was further performed in two typical inert gas atmospheres, i.e. argon gas and nitrogen gas. During experiments, the laser fluence was kept to be 0.235 J/cm^2. Due to the shielding effect of the argon and nitrogen gas on laser energy [47,48], the irradiation time was increased to achieve the equivalent results, 1.9 ms for argon atmosphere and 1.4 ms for nitrogen atmosphere, respectively. Fig. 12 presents the results of GC surface after laser irradiation in the argon and nitrogen atmospheres. It is noted that the similar micro-dimples with ring-like nanostructure on their inner walls have been formed, demonstrating that formation of the hierarchical micro/nano-structure is independent of the gas atmosphere. This indicates that the chemical reaction between the GC and oxygen in air is not the reason for the generated structure.

As the hierarchical micro/nano-structure here mainly includes two features, the micro-dimple and the ring-like nanostructure, their formation mechanisms will be discussed separately, which are illustrated in Fig. 13(a) and (b), respectively. As shown in Fig. 13(a), the laser beam used here has a Gaussian energy distribution. Around the central region, the laser fluence is above the ablation threshold of GC, and thus the GC material in this region is ablated. Being different from the metal materials, GC is a typical carbon material, and the ablated materials will readily react with the surrounding oxygen to generate carbon dioxide. This is why the surrounding of the micro-dimple is quite flat without the commonly observed pile-ups for metal materials [28,49]. At the same time, due to the insufficient combustion of the ablated materials (probably because of the shielding effect of plasma plume that prevents the reaction between ablated material and oxygen), black smoke is

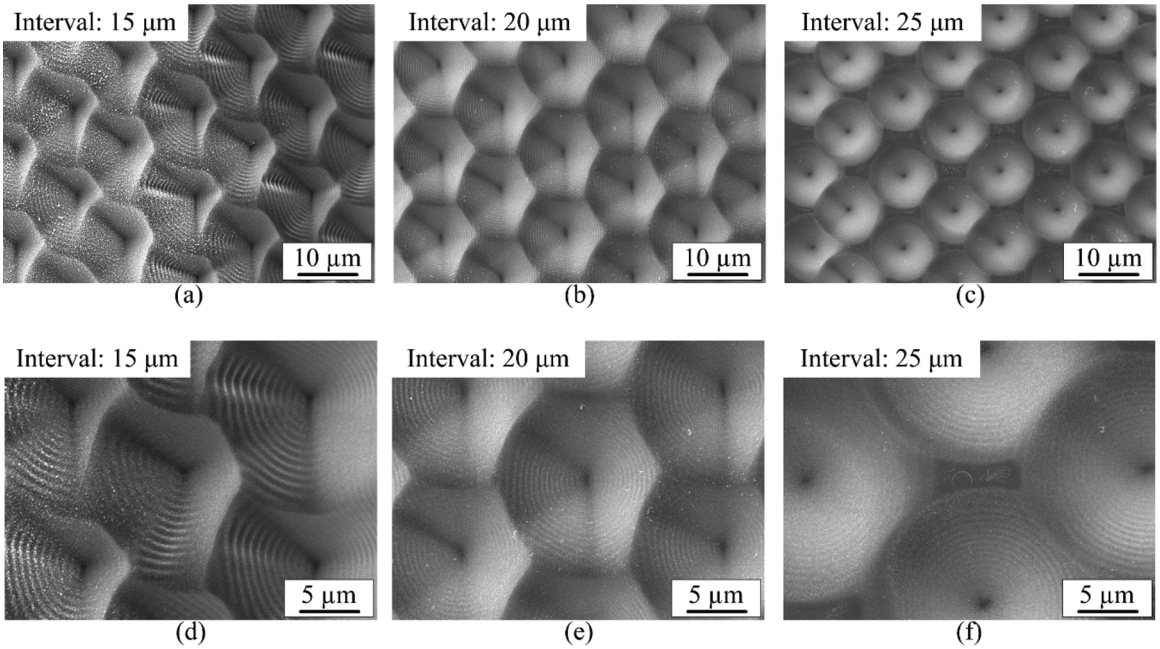

Fig. 8. SEM morphologies of the micro-dimple arrays corresponding to the 3D topographies in Fig. 7: (a, d) interval d =15 μm, (b, e) interval d =20 μm, and (c, f) interval d =25 μm.

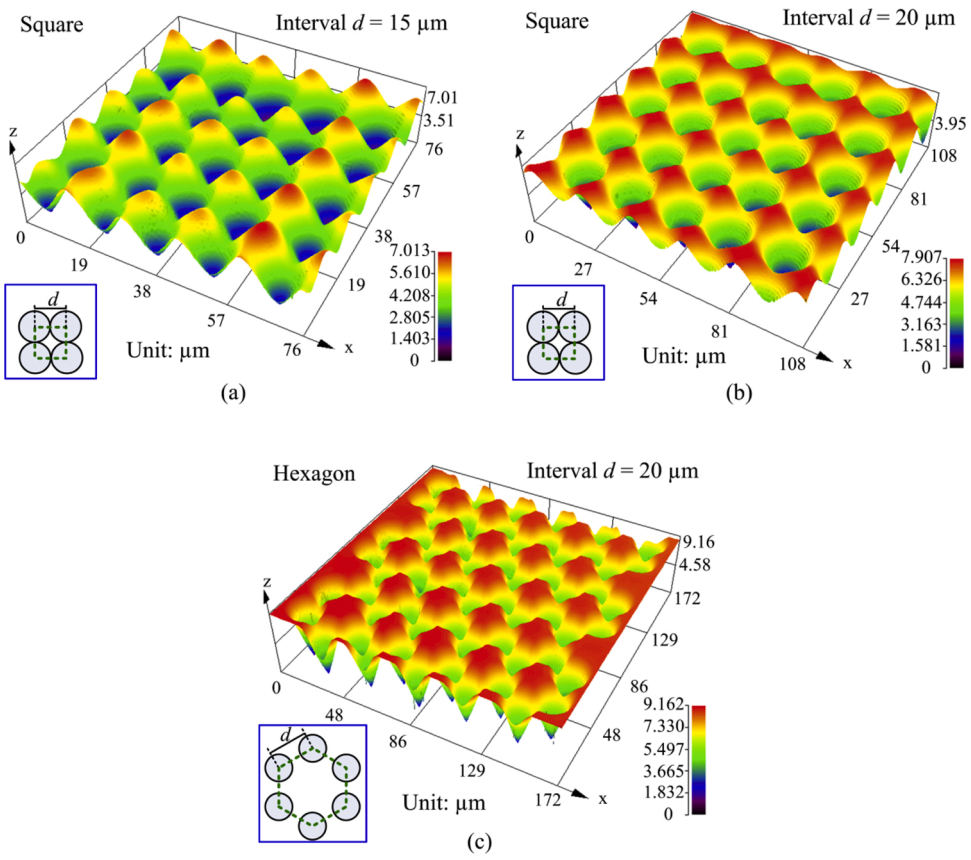

Fig. 9. 3D topographies of the micro-dimple arrays formed by using four points and six points as a basic unit and controlling the interval: (a) four points and d =15 μm, (b) four points and d =20 μm, and (c) six points and d =20 μm.

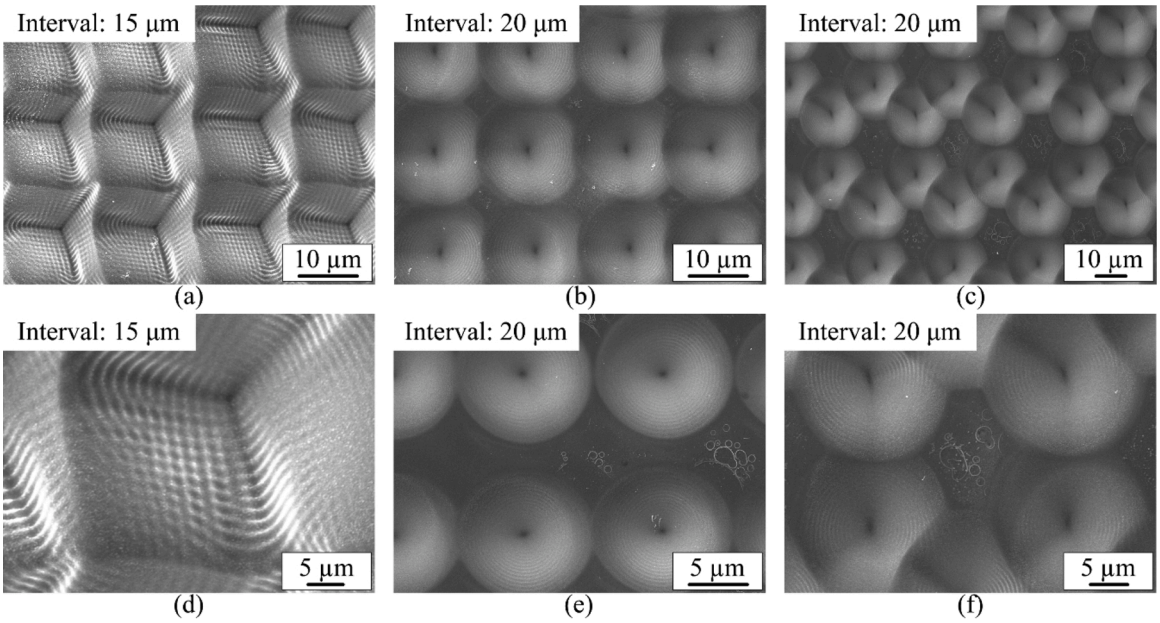

Fig. 10. SEM morphologies of the micro-dimple arrays formed by using four points and six points as a basic unit and controlling the interval: (a, d) four points and d =15 μm, (b, e) four points and d =20 μm, and (c, f) six points and d =20 μm.

experimentally observed. With the role of recoil pressure, the black smoke flows outward and finally produces the nanoparticles around the micro-dimple when the laser is off [27,33,44]. Accordingly, the micro-dimple with Gaussian-like shape and some nanoparticles around is generated on the GC surface after pulsed laser irradiation. In addition, as shown in Fig. 6, due to the crystal anisotropy of graphite, the formed micro-dimple and ring-like nanostructure are quite irregular compared to those formed on the GC surface. This, on the other hand, confirms that the isotropic physical and chemical properties of GC resulting from its amorphous nature should also significantly contribute to the formation

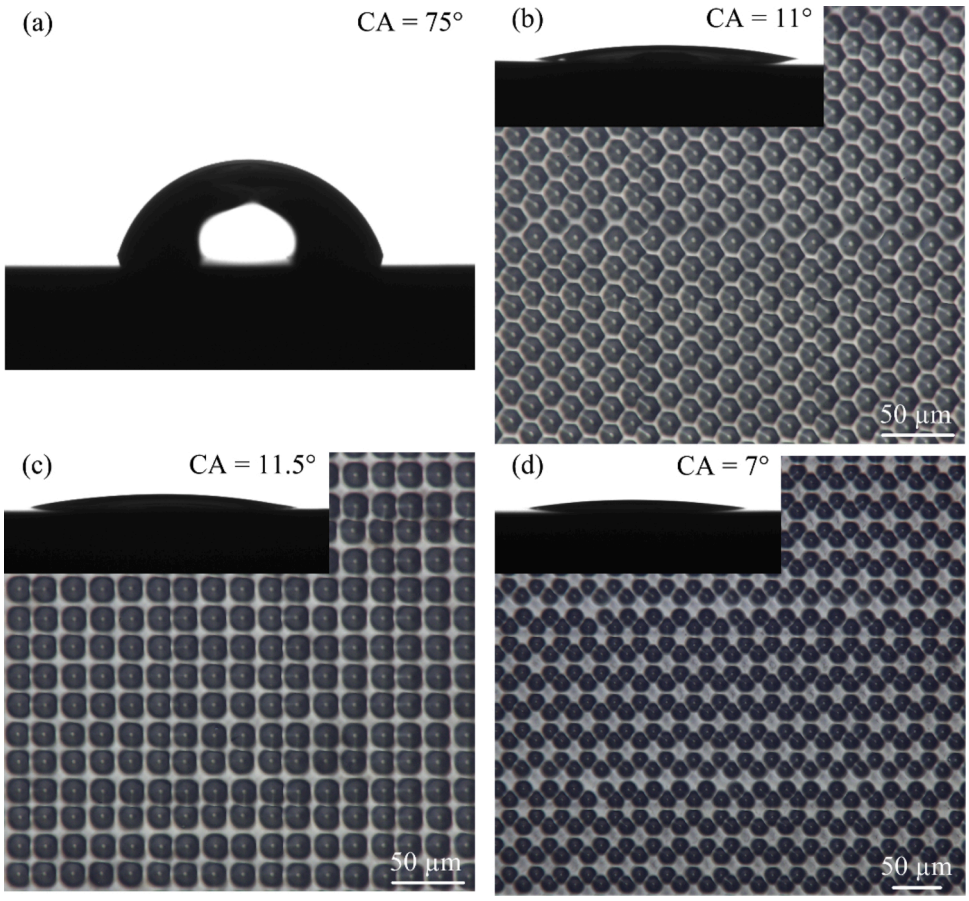

Fig. 11. (a) The contact angle of the original GC surface. (b)-(d) show the optical images and corresponding contact angles of the formed three kinds of micro-dimple arrays. All the intervals were kept to be 20 μm.

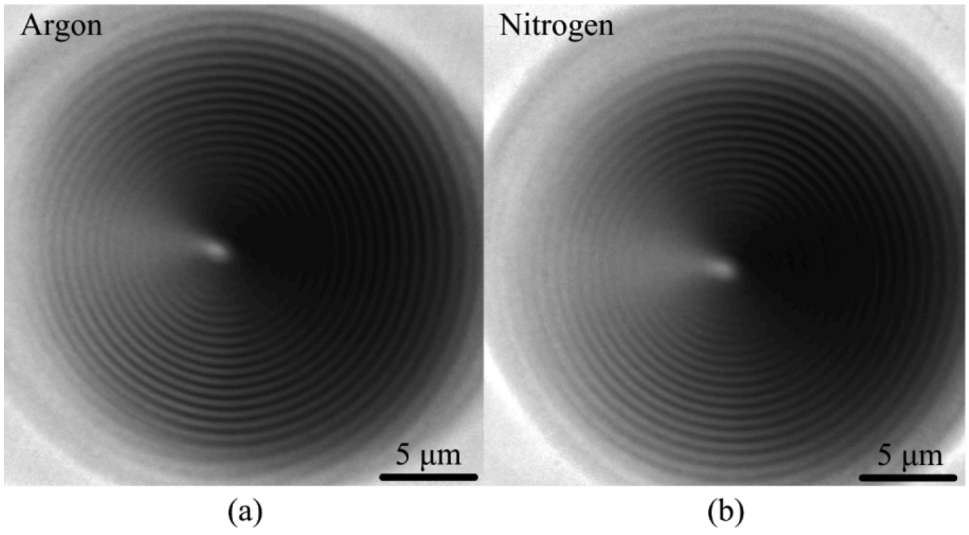

Fig. 12. Optical morphologies of the GC surface after point shot under different atmospheres: (a) argon and (b) nitrogen. The laser fluence was kept to be 0.235 J/cm^2. To generate the similar ring-like nanostructure on the inner wall of the micro-dimple, the irradiation time was increased to 1.9 ms (for argon atmosphere) and 1.4 ms (for nitrogen atmosphere), respectively.

of very regular micro-dimple.

According to the results shown in Fig. 3 and 5, the initial formation of ring-like nanostructure is significantly dependent on the laser irradiation time and fluence, and these two parameters actually determine the same structural parameters of the micro-dimple, i.e., the depth and diameter. From Fig. 4, it is noted that when increasing the laser irradiation time, the change in diameter of the micro-dimple is relatively slight but the depth has been significantly increased. Therefore, the depth of micro-dimple should be the dominant parameter that determines the formation of ring-like nanostructure. That is to say a critical

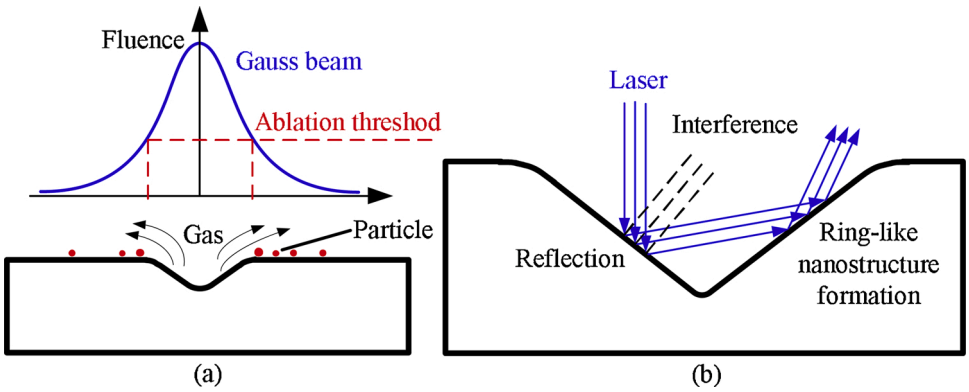

Fig. 13. Schematic diagram illustrating the formation mechanism of the hierarchical micro/nano-structure: (a) formation of the micro-dimple and (b) formation of the ring-like nanostructure.

depth should be reached prior to the formation of ring-like nanostructure. According to some previous studies [33,35,50–53], the formation of ring-like nanostructure could be ascribed to the interference between the incident light and the reflected light. As illustrated in Fig. 13(b), to realize this kind of interference, the reflected light should reach to the inner wall of the micro-dimple. This is why a critical depth should be reached. Accordingly, the possible formation mechanism of ring-like nanostructure is explained as follows. After the irradiation of the first laser pulse, micro-dimple with smooth inner wall could be formed. With increase in the laser pulses (realized by increasing the irradiation time), the micro-dimple could be gradually deepened as shown in Fig. 3 and 4. Once the critical depth is achieved, the reflected light could reach to the inner wall of the micro-dimple, and it further intervenes with the incident light, resulting in the initial formation of the ring-like nanostructure [33,35,50]. When further increasing in the laser pulses, the depth of the ring-like nanostructure could be increased via the increased interference times; therefore, the ring-like nanostructure becomes clearer and clearer, as shown in Fig. 3. After a critical irradiation time (number of laser pulses), damage of the micro-dimple starts from the central region due to the accumulated heat and enhanced absorption of the laser energy around the central region [49,54]. Once the damage is initiated at a precursor, it will expand rapidly with the role of subsequent pulsed laser irradiation [55].

In some previous studies [35,50,52], similar hierarchical micro/nano-structures have been reported for SiO_2 thin film, ZnO, fused silica, et al. by using nanosecond and femtosecond lasers. Compared to these studies, the formed micro-dimple and ring-like nanostructure here are quite regular and clean with extremely less defects. This could benefit from the carbon material and amorphous nature of GC. The regular and clean micro/nano-structure would endow the GC more functional applications.

4. Conclusions

In summary, this paper reported a one-step method for fabricating hierarchical micro/nano-structures on the GC surface by nanosecond pulsed laser irradiation. Via experiments and analysis, the following conclusions can be derived.

(1) A typical hierarchical micro/nano-structure, i.e., micro-dimple with ring-like nanostructure on its inner wall, could be generated on the GC surface through point shot by using the nanosecond pulsed laser.
(2) Formation of the ring-like nanostructure strongly depended on the laser irradiation time and fluence, and these two parameters showed a similar effect. To obtain a regular ring-like nanostructure, these two parameters should be experimentally selected.
(3) The formation of very regular hierarchical micro/nano-structure benefited from the amorphous nature of GC and it was independent of the used gas atmosphere.
(4) By controlling the relative positions of point shots, various micro-dimple arrays were fabricated on the GC surface, which significantly changed the surface wetting behavior.

Declaration of Competing Interest

The authors declare that they have no known competing financial interests or personal relationships that could have appeared to influence the work reported in this paper.

Acknowledgments

This work was supported by the National Natural Science Foundation of China (Grant No. 51705197), the Young Elite Scientists Sponsorship Program by CAST (YESS) (Grant No. 2017QNRC001), the Graduate Innovation Fund of Jilin University (Grant No. 101832020CX106), and the Fundamental Research Funds for the Central Universities (2019-2021).

References

[1] Bauer J, Schroer A, Schwaiger R, Kraft O. Approaching theoretical strength in glassy carbon nanolattices. Nat Mater 2016;15(4):438–43.
[2] Zhang F, Ilavsky J, Long GG, Quintana JPG, Allen AJ, Jemian PR. Glassy carbon as an absolute intensity calibration standard for small-angle scattering. Metall Mater Trans A 2009;41(5):1151–8.
[3] Li X, Gao H. Smaller and stronger. Nat Mater 2016;15(4):373–4.
[4] Hu M, He J, Zhao Z, Strobel TA, Hu W, Yu D. Compressed glassy carbon: an ultrastrong and elastic interpenetrating graphene network. Sci Adv 2017;3:1603213.
[5] Prater K, Dukwen J, Scharf T, Herzig HP, Plöger S, Hermerschmidt A. Microstructuring of glassy carbon for precision glass molding of binary diffractive optical elements. Opt Mater Express 2016;6(11):3407–16.
[6] Nam E, Lee C-Y, Jun MBG, Min B-K. Ductile mode electrochemical oxidation assisted micromachining for glassy carbon. J Micromech Microeng 2015;25(4):045021.
[7] Beiring P, Yan J. Ultrasonic vibration-assisted microgrinding of glassy carbon. P I Mech Eng C-J Mec 2019;233(12):4165–75.
[8] Youn SW, Takahashi M, Goto H, Maeda R. Fabrication of micro-mold for glass embossing using focused ion beam, femto-second laser, eximer laser and dicing techniques. J Mater Process Tech 2007;187-188:326–30.
[9] Youn SW, Ueno A, Takahashi M, Maeda R. A process of glassy carbon etching without the micro masking effect for the fabrication of a mold with a high-quality surface. J Micromech Microeng 2009;19(12):125010.
[10] Kim J, Hong D, Badshah MA, Lu X, Kim YK, Kim SM. Direct metal forming of a microdome structure with a glassy carbon mold for enhanced boiling heat transfer. Micromachines (Basel) 2018;9(8). https://doi.org/10.3390/mi9080376.
[11] Hu Chopra P. Fibre laser machining for glassy carbon master mould and soft lithography based two-step printing for Ag nanoparticle structures. Opt Laser Eng 2011;49(4):498–506.
[12] Tseng SF, Chen MF, Hsiao WT, Huang CY, Yang CH, Chen YS. Laser micromilling of convex microfluidic channels onto glassy carbon for glass molding dies. Opt Laser Eng 2014;57:58–63.

[13] Krishnan DV, Kumar GU, Suresh S, Jubal M, Thansekhar MR, Ramesh R. Wetting transition in laser-fabricated hierarchical surface structures and its impact on condensation heat transfer characteristics. Int J Heat Mass Transf 2019;140:886–96.
[14] Samanta A, Huang W, Chaudhry H, Wang Q, Shaw SK, Ding H. Design of chemical surface treatment for laser-textured metal alloys to achieve extreme wetting behavior. ACS Appl Mater Interfaces 2020;12(15):18032–45.
[15] Chen H, Zhang P, Zhang L, Liu H, Jiang Y, Zhang D, et al. Continuous directional water transport on the peristome surface of Nepenthes alata. Nature 2016;532(7597):85–9.
[16] Wang Q, Samanta A, Shaw SK, Hu H, Ding H. Nanosecond laser-based high-throughput surface nanostructuring (nHSN). Appl Surf Sci 2020;507:145136.
[17] Fan P, Bai B, Zhong M, Zhang H, Long J, Han J, et al. General strategy toward dual-scale-controlled metallic micro-nano hybrid structures with ultralow reflectance. ACS Nano 2017;11(7):7401–8.
[18] Chen X, Wu J, Ma R, Hua M, Koratkar N, Yao S, et al. Nanograssed micropyramidal architectures for continuous dropwise condensation. Adv Funct Mater 2011;21(24):4617–23.
[19] Hou YM, Yu M, Chen XM, Wang ZK, Yao SH. Recurrent filmwise and dropwise condensation on a beetle mimetic surface. ACS Nano 2015;9(1):71–81.
[20] Long J, He Z, Zhou P, Xie X, Zhou C, Hong W, et al. Low-cost fabrication of large-area broccoli-like multiscale micro- and nanostructures for metallic super-hydrophobic surfaces with ultralow water adhesion and superior anti-frost ability. Adv Mater Interfaces 2018;5(13):1800353.
[21] Grützmacher PG, Profito FJ, Rosenkranz A. Multi-scale surface texturing in tribology—current knowledge and future perspectives. Lubricants 2019;7(11). https://doi.org/10.3390/lubricants7110095.
[22] Grützmacher PG, Rosenkranz A, Szurdak A, König F, Jacobs G, Hirt G, et al. From lab to application - improved frictional performance of journal bearings induced by single- and multi-scale surface patterns. Tribol Int 2018;127:500–8.
[23] He A, Liu WW, Xue W, Yang H, Cao Y. Nanosecond laser ablated copper superhydrophobic surface with tunable ultrahigh adhesion and its renewability with low temperature annealing. Appl Surf Sci 2018;434:120–5.
[24] Ta DV, Dunn A, Wasley TJ, Kay RW, Stringer J, Smith PJ, et al. Nanosecond laser textured superhydrophobic metallic surfaces and their chemical sensing applications. Appl Surf Sci 2015;357:248–54.
[25] Nürnberger P, Reinhardt HM, Kim H-C, Pfeifer E, Kroll M, Müller S, et al. Orthogonally superimposed laser-induced periodic surface structures (LIPSS) upon nanosecond laser pulse irradiation of SiO_2/Si layered systems. Appl Surf Sci 2017;425:682–8.
[26] Jagdheesh R, Garcia-Ballesteros JJ, Ocana JL. One-step fabrication of near superhydrophobic aluminum surface by nanosecond laser ablation. Appl Surf Sci 2016;374:2–11.
[27] Huang H, Jun N, Jiang M, Ryoko M, Yan J. Nanosecond pulsed laser irradiation induced hierarchical micro/nanostructures on Zr-based metallic glass substrate. Mater Des 2016;109:153–61.
[28] Williams E, Brousseau EB. Nanosecond laser processing of Zr41.2 Ti13.8 Cu12.5 Ni10 Be22.5 with single pulses. J Mater Process Tech 2016;232:34–42.
[29] Nasser J, Lin J, Zhang L, Sodano HA. Laser induced graphene printing of spatially controlled super-hydrophobic/hydrophilic surfaces. Carbon 2020;162:570–8.
[30] Veiko V, Karlagina Y, Moskvin M, Mikhailovskii V, Odintsova G, Olshin P, et al. Metal surface coloration by oxide periodic structures formed with nanosecond laser pulses. Opt Laser Eng 2017;96:63–7.
[31] Klotzbach U, Washio K, Kling R, Lasagni AF, Gachot C, Trinh KE, et al. Direct laser interference patterning, 20 years of development: from the basics to industrial applications. Laser-based micro- and nanoprocessing XI. Proc. of SPIE 10092:1-11 2017.
[32] Rosenkranz A, Hans M, Gachot C, Thome A, Bonk S, Mücklich F. Direct laser interference patterning: tailoring of contact area for frictional and antibacterial properties. Lubricants 2016;4(1). https://doi.org/10.3390/lubricants4010002.
[33] Takayama N, Yan J. Mechanisms of micro-groove formation on single-crystal diamond by a nanosecond pulsed laser. J Mater Process Tech 2017;243:299–311.
[34] Huang H, Yan J. Surface patterning of Zr-based metallic glass by laser irradiation induced selective thermoplastic extrusion in nitrogen gas. J Micromech Microeng 2017;27(7).
[35] Sun W, Qi H, Fang Z, Yu Z, Liu Y, Yi K, et al. Nanosecond laser pulse induced concentric surface structures on SiO_2 layer. Opt Express 2014;22(3):2948.
[36] Nathan MI, Smith JE, Tu KN. Raman spectra of glassy carbon. J Appl Phys 1974;45(5):2370.
[37] Ferrari AC, Robertson J. Interpretation of Raman spectra of disordered and amorphous carbon. Phys Rev B 2000;61(20):14095–107.
[38] Taylor SM, Pătru A, Streich D, El Kazzi M, Fabbri E, Schmidt TJ. Vanadium (V) reduction reaction on modified glassy carbon electrodes – role of oxygen functionalities and microstructure. Carbon 2016;109:472–8.
[39] Komlenok MS, Arutyunyan NR, Kononenko VV, Zavedeev EV, Frolov VD, Chouprik AA, et al. Structure and friction properties of laser-patterned amorphous carbon films. Diam Relat Mater 2016;65:69–74.
[40] Mustafa H, Mezera M, Matthews DTA, Römer GRBE. Effect of surface roughness on the ultrashort pulsed laser ablation fluence threshold of zinc and steel. Appl Surf Sci 2019;488:10–21.
[41] Nieto D, Arines J, O'Connor GM, Flores-Arias MT. Single-pulse laser ablation threshold of borosilicate, fused silica, sapphire, and soda-lime glass for pulse widths of 500 fs, 10 ps, 20 ns. Appl Opt 2015;54(29):8596–601.
[42] Janicijevic M, Sreckovic M, Kaludjerovic B, Dinulovic M, Karastojkovic Z, Jovanic P, et al. Evaluation of laser beam interaction with carbon based material - glassy carbon. Chem Ind Chem Eng Q 2015;21(1–1):63–9.
[43] Bulgakova NM, Bulgakov AV. Pulsed laser ablation of solids: transition from normal vaporization to phase explosion. Appl Phys A-Mater 2001;73(2):199–208.
[44] Liu X, Shen H, Liu J, Zhang J, Chen Y, Zhang Z, et al. A green, maskless, and universal preparation method for patterned surfaces on various metal substrates. Appl Surf Sci 2020;514:145838.
[45] Wang D, Sun Q, Hokkanen MJ, Zhang C, Lin FY, Liu Q, et al. Design of robust superhydrophobic surfaces. Nature 2020;582(7810):55–9.
[46] Samanta A, Wang Q, Shaw SK, Ding H. Roles of chemistry modification for laser textured metal alloys to achieve extreme surface wetting behaviors. Mater Design 2020:192.
[47] Zinovik I, Povitsky A. Dynamics of multiple plumes in laser ablation: modeling of the shielding effect. J Appl Phys 2006;100(2):024911.
[48] Xu J, Luo Y, Zhu L, Han J, Zhang C, Chen D. Effect of shielding gas on the plasma plume in pulsed laser welding. Measurement 2019;134:25–32.
[49] Lu G, Sokol DW, Zhang Y, Dulaney JL. Nanosecond pulsed laser-generated stress effect inducing macro-micro-nano structures and surface topography evolution. Appl Mater Today 2019;15:171–84.
[50] Song J, Qian B, Xu J, Guo X, Qiu J. Simultaneous formation of two types of periodic nanostructure in ZnO single crystal by femtosecond laser direct irradiation. Jpn J Appl Phys 2010;49(11):112001.
[51] Trtica MS, Gakovic BM, Radak BB, Batani D, Desai T, Bussoli M. Periodic surface structures on crystalline silicon created by 532nm picosecond Nd:YAG laser pulses. Appl Surf Sci 2007;254(5):1377–81.
[52] Zhang X, Jiang Y, Qiu R, Meng J, Cao J, Zhang C, et al. Concentric ring damage on the front surface of fused silica induced by a nanosecond laser. Opt Mater Express 2019;9(12):4811.
[53] Liu D, Chen C, Man B, Meng X, Sun Y, Li F. Evolution and mechanism of the periodical structures formed on Ti plate under femtosecond laser irradiation. Appl Surf Sci 2016;378:120–9.
[54] Yu J, Xiang X, He S, Yuan X, Zheng W, Lü H, et al. Laser-induced damage initiation and growth of optical materials. Adv Cond Matter Phys 2014;2014:1–10.
[55] Negres RA, Norton MA, Cross DA, Carr CW. Growth behavior of laser-induced damage on fused silica optics under UV, ns laser irradiation. Opt Express 2010;18:19966–76.